Efficient Focusing with Large Numerical Aperture Using a Hybrid Metalens

Ming Kang,[1,†] Younes Ra'di,[1,2,†] Diego Farfan,[1] and Andrea Alù[1,2,3,4,*]

[1] *Department of Electrical and Computer Engineering, The University of Texas at Austin, Austin, Texas 78712, USA*

[2] *Photonics Initiative, Advanced Science Research Center, City University of New York, New York 10031, USA*

[3] *Physics Program, Graduate Center, City University of New York, New York 10016, USA*

[4] *Department of Electrical Engineering, City College of The City University of New York, New York 10031, USA*

(Received 23 October 2019; revised manuscript received 1 March 2020; accepted 18 March 2020; published 7 April 2020)

Focusing light using electrically thin layers is of paramount importance in several applications, from integrated optics to microwave engineering and sensing. Recently, gradient metasurfaces, which are electrically thin arrays of densely located polarizable particles, have been employed to perform different wave-front transformations, including focusing. In comparison to a bulk lens, these designs provide ultrathin geometries, but they suffer from fundamental limitations on their overall efficiency and achievable numerical aperture. Metagratings offer a solution for efficient beam steering at large angles, but it is challenging to utilize them in the small-angle limit. Here, we introduce a hybrid metalens design, which provides dramatic enhancement in lensing performance compared with that of state-of-the-art metasurfaces, combining metagratings and conventional gradient approaches. Our experimental prototype enables microwave focusing with large efficiency ($\eta = 0.479$) and near-unity numerical aperture (NA $= 0.98$), yielding a sharp focal point at the diffraction limit in the far field (FWHM $= 0.332\lambda$). We propose a hybrid metalens design with exceptional performance in terms of efficiency and numerical aperture, opening up opportunities for high-throughput optical lithography, high-density data recording, focal plane arrays, radar, and communication systems.

DOI: 10.1103/PhysRevApplied.13.044016

I. INTRODUCTION

Controlling the electromagnetic wave front in terms of phase, amplitude, and polarization is at the basis of several technologies of widespread use, from imaging and sensing devices to radars and communication systems. The conventional approach to wave-front manipulation relies on bulk devices, much larger than the wavelength, in which the transformation occurs gradually along the optical path. This is the core design principle behind common lenses, resulting in structures with input and output interfaces that need to be precisely engineered [1]. Although these structures can efficiently focus and image, their size is a significant limiting factor for several applications. This issue becomes even more imposing at microwave frequencies, for which the size of these devices scales with the wavelength, leading to very bulky devices for focusing and beam steering.

These challenges have been tackled in the metamaterials community using various approaches [2]. Volumetric metamaterials, with exotic refractive indexes, can implement lenses with improved properties and smaller footprint, e.g., Maxwell fish-eye and Luneburg lenses [3–5]. However, fabrication complexity, increased loss, and narrow bandwidths have hampered the use of volumetric metamaterial lenses.

Metasurfaces, which are the planarized version of metamaterials, provide a powerful platform to control the flow of light within electrically thin layers [6–8]. They are typically formed by two-dimensional arrays of closely located scatterers with spatially varying properties, which can perform a wide range of wave-front transformations with large flexibility and subwavelength resolution. Gradient metasurfaces, as one of the most popular classes of these engineered surfaces, locally reroute the direction of the incident wave by imparting momentum to the incoming beam through the local gradient of the surface impedance [9], leveraging a spatially varying phase profile to imprint the required wave-front transformation in reflection and/or transmission [10–16]. This approach provides a rich platform to design different types of electrically thin lenses [16–22]. However, these designs typically suffer from low efficiency, small numerical aperture, and/or electrically large focal points. Although, different attempts have been

*aalu@gc.cuny.edu

†These authors contributed equally to this work.

made to address these issues, there is a clear trade-off between total efficiency and numerical aperture, implying high efficiency at the cost of low numerical aperture [23] or near-unity numerical aperture at the cost of low efficiencies (e.g., Ref. [24]).

To understand the fundamental limitations of gradient metasurface lenses, let us consider a metalens designed, based on the generalized laws of reflection and refraction [9], to focus a normally incident wave into a focal point located above the center of the lens. For points over the metasurface located farther away from the focus, the steering angle becomes larger. This issue is more pronounced for lenses with near-unity numerical aperture, for which the lens edges are responsible for steering the incident wave at angles close to 90°. It has been recently shown that there is a fundamental physical limit on the steering efficiency of gradient metasurfaces, which degrades rapidly as the angle becomes close to 90° [25–27]. Thus, gradient metasurface lenses with high numerical aperture perform poorly far from the center of the lens, and, after some point, increasing the size of the lens will no longer improve the lens efficiency.

Metagratings can address this challenge, enabling beam steering at extreme angles with unitary efficiency [28]. Metagratings are periodic arrays of scatterers, in which the periodicity is chosen to open higher Floquet channels, as in a regular grating. By aligning one of them with the desired steering direction and designing the scatterer to create nulls of radiation in the undesired Floquet channel directions, the incident wave can be fully redirected towards an arbitrary direction with unitary efficiency [28–35]. Designing a lens based on such a structure would naturally enable lenses with high efficiency and near-unity numerical aperture. However, metagratings suffer from two problems, relative to gradient metasurfaces: for steering angles smaller than 30°, unwanted higher-order Floquet channels appear, and the closer we get to specular reflection, the larger the number of these channels becomes. This implies that unit-cell engineering can become overly complicated to make sure that many scattering nulls are suitably located to suppress these undesired Floquet channels. Conventional gradient metasurfaces can tackle well the task of redirecting the beams for small angles; therefore, an optimal solution for the design of efficient metalenses is to combine the two approaches, envisioning a hybrid design employing the gradient approach for areas of the lens around the focus and the metagrating approach for areas closer to the edges.

Here, we explore and implement a hybrid metalens based on this principle, capable of providing high efficiency, near-unity numerical aperture, and hence, a very tight focal point. Our prototype offers a measured total efficiency of $\eta = 0.479$, a numerical aperture of 0.98, and a smaller focal point with a full width at half maximum of FWHM $= 0.332\lambda$.

II. HYBRID METALENS

A. Design, numerical simulations, and experimental validation

Figure 1(a) shows the schematic of our hybrid metalens, which is composed of two different regions: a central portion designed based on the gradient approach and the metagrating regions around it. For simplicity, we focus on a reflective metalens design operating in one dimension (the metasurface is invariant in the y direction). Here, as a proof of concept, we design and experimentally demonstrate a hybrid metalens for 22.4 GHz; however, the same design approach is scalable to different portions of the electromagnetic spectrum, up to the visible range. To design the gradient metasurface portion of the lens, we follow the conventional approach that ignores impedance mismatch (which is small because of the nonextreme steering angles) and focuses on locally manipulating the reflection phase based on the generalized law of reflection [9]. It can be easily shown that the local reflection phase shift required at every point over the surface, to reflect a normally incident beam towards the focal point, is $\Phi = (2\pi/\lambda)\left(\sqrt{x^2 + l_{\text{foc}}^2} - l_{\text{foc}}\right)$ [7], where λ is the wavelength of the incident wave and l_{foc} is the focal distance of the lens. For our example, we assume $l_{\text{foc}} = 40\,\text{mm} \approx 3\lambda$.

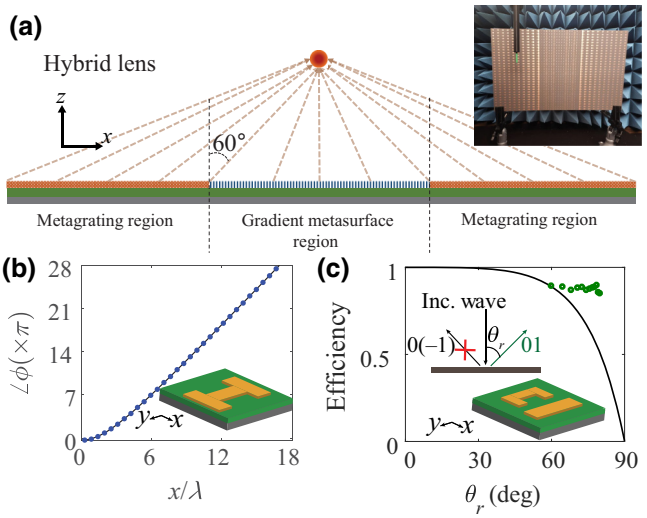

FIG. 1. Hybrid metalens composed of gradient metasurface and metagrating regions. (a) Schematic of the hybrid metalens. Right inset shows the fabricated hybrid metalens and experimental setup. (b) Desired phase profile for the gradient metasurface region (solid line) and designed metasurface elements (circles). Inset shows the schematic of our unit-cell design. (c) Fundamental limit on the conversion efficiency of a reflective gradient metasurface [25–27] (solid line) and the predicted efficiency, including material loss, for metagratings designed for beam steering towards extreme angles (green dots). Inset shows the schematic of our unit-cell design.

The required phase profile for this configuration is shown in Fig. 1(b). We design each unit cell by neglecting the phase variations along the surface, which are slow, and by assuming a local periodicity aimed at steering the beam in the required direction, providing the required phase shift as a function of its position along x, as shown in Fig. 1(b). For the sake of simplicity, we keep the unit-cell size the same in this region (e.g., $c_x \times c_y = 0.56\lambda \times 0.6\lambda$) and achieve the required phase profile by simply tuning the dimensions of the inclusion inside the unit cells. The surface is periodic in the y direction with subwavelength periodicity c_y to prevent additional Floquet channels propagating in this plane. The building block scatterer used for this region is shown in the inset of Fig. 1(b). In all our numerical simulations throughout the paper, we consider realistic loss in the involved materials (the substrate material is DiClad 880 with a permittivity of 2.2 and a loss tangent a 0.0009, and realistic copper is used as the metallic pattern). The detailed design procedure together, with all design parameters, are provided in Appendix A. As we move away from the center of the lens, the required steering angle grows and, as a result, the gradient metasurface efficiency drops, with a dependence on the steering angle plotted in Fig. 1(c) [25–27]. We choose the boundary between the gradient and metagrating regions to be the region with a steering angle at 60°, as shown in Fig. 1(a), since, at this angle, the gradient approach can still provide a reasonably high efficiency.

The design of the metagrating unit cells is inspired by Ref. [28]: we choose the local periodicity $q_x = \lambda/\sin\theta_r$, so that the -1 and $+1$ higher-order Floquet channels enter the light cone and one of them is aligned towards the focal point direction. Next, we design a single scatterer in each unit cell, so that the reflected fields towards all open channels, except the one aligned with the desired steering direction, are cancelled [see the inset of Fig. 1(c)]. The efficiency of the designed metagrating unit cells, as a function of the steering angle, together with a sketch of the unit cell implemented for this region of the metalens, are shown in Fig. 1(c), considering the same substrate as that in the central gradient region. As observed from this plot, the efficiency of these structures lies well above the bound of conventional gradient metasurfaces. Notably, in principle, the efficiencies of the designed metagratings can be unitary; however, since here we consider realistic structures with ohmic loss, the efficiencies drop to around 90%. Here, 10% of the incident wave is lost in the form of scattering into undesired channels and dissipation due to the presence of loss in the structure. Notably, by further optimizing these designs, the grating efficiency can be increased. Similar to the gradient metasurface region, ideally, our design assumes an infinite metagrating array at every location over the surface of the metalens, which would enable the incident wave to be locally reflected in the desired direction of reflection. However, due to limited space, we use only one unit cell as a representative of each array. Therefore, on the metagrating regions, we have several unit cells with different unit-cell periods, q_x, each representative of the corresponding metagrating aimed at locally reflecting towards the focus. Given that the reflection angle does not change dramatically across the lens, this approximation works well in the final design of the lens. The total size of the designed lens is 30.2λ, which includes 16 elements in the gradient metasurface region and 20 elements in the two metagrating regions. A detailed design procedure, together with all the design parameters, are given in Appendix B.

To experimentally validate our design of a hybrid metalens, we fabricate a prototype for operation at 22.4 GHz, as shown in the inset of Fig. 1(a) (a clearer picture of the fabricated hybrid metalens is given in Fig. 7 within Appendix C). Full-wave simulation and measurement results for the designed lens are shown in Fig. 2 (details regarding the measurement setup are given in Appendix C). Figures 2(a) and 2(b) show the simulated and measured intensity of the reflected electric field normalized to the intensity of the incident one, respectively, demonstrating that the structure can efficiently focus the incident wave at the focal point (i.e., $x = 0, z = 3.1\lambda$). Notably, the measured focal length is 3.1λ, which is slightly larger than that of the predicted value, i.e., $l_{\text{foc}} \approx 3\lambda$. Figures 2(c) and 2(d) show two different cuts of Figs. 2(a) and 2(b) at $z = 3.1\lambda$ and $x = 0$, respectively. The calculated numerical aperture of the lens is NA ≈ 0.98, and the full width at half maximum at the

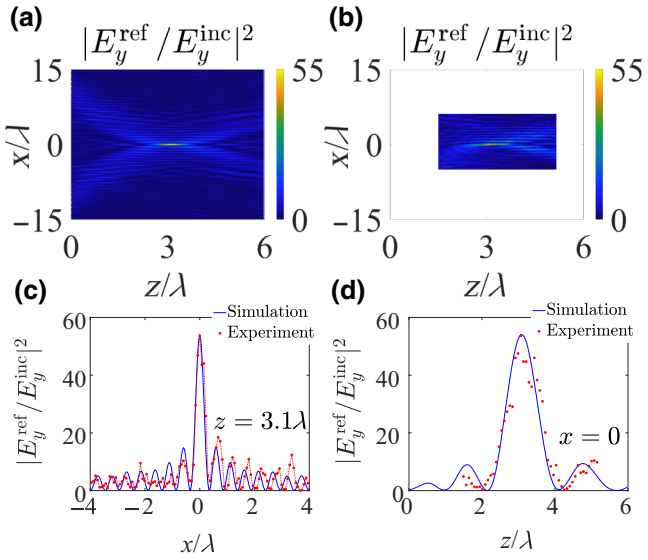

FIG. 2. Performance of the hybrid metalens. (a) Numerical and (b) experimental field intensity map of the designed hybrid metalens around the focus. (c) Numerical (solid line) and experimental (circles) reflected field intensity at the focal point (i.e., $z = 3.1\lambda$) for the hybrid metalens. (d) Numerical (solid line) and experimental (circle) reflected field intensity at $x = 0$.

focal point is FWHM $= 0.332\lambda$. As observed from the results presented in Fig. 2, the numerical and experimental results are in a very good agreement. To evaluate the efficiency, η, of the metalens, different definitions have been proposed in the recent literature [18–24]. Here, we define the efficiency as that in Ref. [21], i.e., as the fraction of incident light that passes through a slit in the focal plane with width equal to 6 times the FWHM. For our design, $\eta = 0.479$, which is a very large value for a metalens with near-unity numerical aperture and small focal point (notably, only 0.8% of the illuminated power is absorbed due to the presence of the dissipative loss in the structure). These results show remarkable performance in comparison to that of recently reported results. For example, in contrast with the results presented in Ref. [24], our results demonstrate a significant increase in focusing efficiency within a smaller focal region. It should be noted that different efficiency definitions have been utilized by different authors, which can be a source of confusion when comparing the performance of different designs. Throughout our paper, we utilize the definition given in Ref. [21], which is a more meaningful definition and is a well-accepted definition in the community. For example, if we employ the definition used in Ref. [36], our proposed design would have 95.3% efficiency at NA $= 0.98$, while the design presented in Ref. [36] has 79% efficiency at NA $= 0.94$, proving that our proposed design has a much better performance. Quite remarkably, in the design process, we simply apply the design principles stemming from our analytical approach to design the hybrid metalens without any further global optimization. Hence, we expect that improved results can be achieved with further overall structure optimization starting from this design.

A slight deviation between measurement and numerical results can be attributed to the fact that excitation at the location of the sample is not an ideal plane wave and the angle of incidence is slightly deviated from the normal direction in the x-z plane to enable the scanning operation. Any variation of the incident angle from the normal will disturb the operation of unit cells in both gradient and metagrating regions of the hybrid metalens. To verify the sensitivity of the lens to the deviation of the incident angle, we study the operation of the lens for two cases in which the incidence angle is deviated from the normal, i.e., 4° and 8° incidence cases (see Fig. 3). It can be seen that, as the incidence angle grows, more distortion is observed in the focusing operation. Frequency dispersion and chromatic aberrations are other important factors in the performance of a lens. Due to the nature of the design based on diffraction optics, frequency dispersion is naturally expected. However, the overall performance, such as FWHM and overall efficiency, shows quite stable behavior in comparison to that of conventional gradient metalens designs. Namely, a 6% decrease in the frequency of illumination shifts the focal point towards the hybrid metalens, as expected, but the focal area stays considerably small and the total efficiency of the structure drops only slightly, i.e., $\eta = 0.352$ (more details are provided in Appendix D).

III. COMPARISON BETWEEN THE HYBRID METALENS AND GRADIENT METALENS DESIGNS

In Sec. II, we present the concept and experimental implementation of a hybrid metalens that enables efficient focusing with a large numerical aperture and small focal spot size. Here, we compare the lenses based on the proposed concept with conventional metasurface lenses. Figure 4(a) shows two different lenses that are designed to focus a normally incident wave in reflection with a focal length of $l_{\text{foc}} \approx 3\lambda$. The upper panel in Fig. 4(a) shows the hybrid metalens, while the lower panel shows a schematic

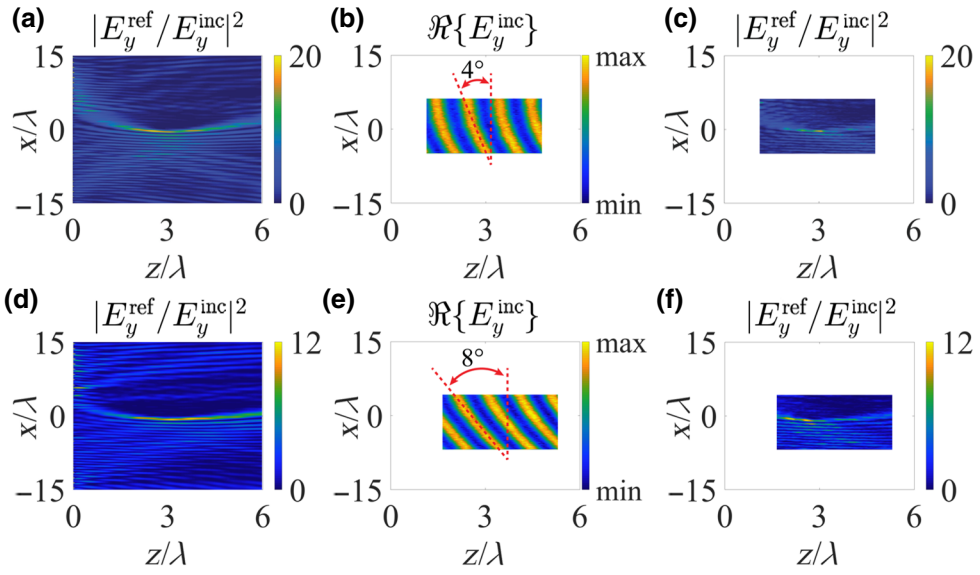

FIG. 3. Numerical and experimental focusing performance of the hybrid metalens at 4° oblique incidence. (a) Normalized reflected field intensity (simulation), (b) real part of the incident field in the scanned region (experiment), and (c) normalized reflected field intensity (experiment). Numerical and experimental focusing performance of the hybrid metalens at 8° oblique incidence. (d) Normalized reflected field intensity (simulation), (e) real part of the incident field in the scanned region (experiment), and (f) normalized reflected field intensity in the scanned region (experiment).

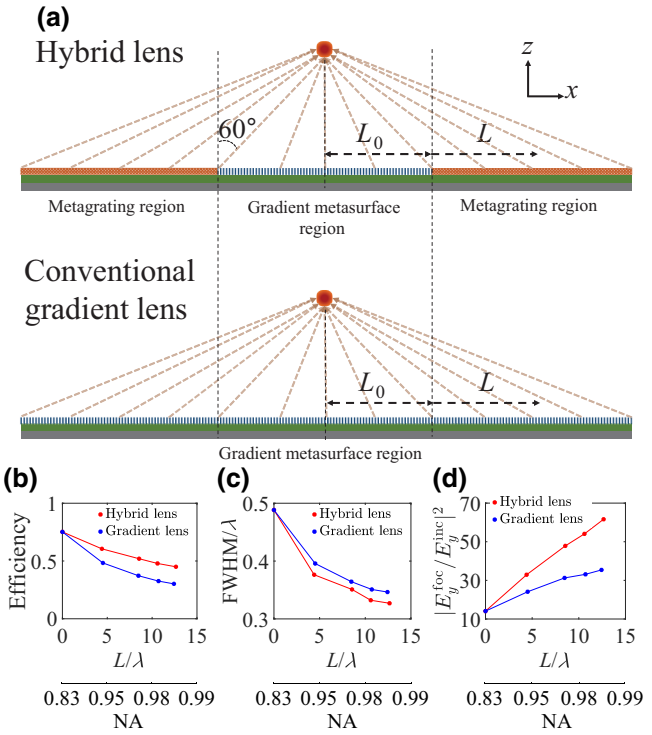

FIG. 4. Comparison between the hybrid metalens and a conventional gradient metalens. (a) Schematic of the hybrid metalens (upper panel) and conventional gradient lens (lower panel). Comparison of (b) efficiency, (c) FWHM, and (d) intensity of the reflected field at the focal point between the hybrid metalens and gradient metalens for different lens apertures.

of a conventional gradient lens designed over its entire aperture based on the concept of the generalized law of reflection and refraction. For a fair comparison, we assume that the two lenses have the same size. Figures 4(b)–4(d) compare the FWHM, efficiency η, and intensity of the electric field at the focal point normalized to the incident field for the two approaches. For $L = 0$, the two designs are identical (two conventional gradient lenses with half-length $L_0 \approx 4.51\lambda$), which naturally results in the two designs having the same properties [Figs. 4(b)–4(d)]. As we increase L, however, enlarging the region in which we use the metagrating approach in the hybrid lens, we achieve considerably better performance than that of the conventional gradient metalenses. Interestingly, there is no trade-off in the observed performance improvement, and for any given aperture, all properties of the proposed design are better than those in the conventional design approach. For example, for the largest lens size considered in this analysis, the hybrid metalens concept provides 15% higher efficiency than that of the conventional design. In addition to the higher focusing efficiency, the hybrid metalens obtains a smaller size of the focusing point than that of the conversional metalens, as shown in Fig. 4(c). For the hybrid metalens design, higher efficiency and smaller focusing point enable a peak intensity larger than that of the conventional lenses, as shown in Fig. 4(d). In all of these results, realistic loss has been considered to provide a fair comparison between two designs. The improved performance for the hybrid metalens is clearly associated with the superior steering capability for large angles of the metagrating approach, which makes better use of the regions of the lens closer to the edges.

IV. CONCLUSIONS

Here, we present a hybrid approach to the design of metalenses, taking the best of both gradient metasurfaces and metagrating approaches, enabling focusing with high performance from a metasurface. Our hybrid metalens is composed of a regular gradient metasurface in its central region, while the outer regions closer to the edges employ the concept of metagratings. Our results show improved performance compared with that of conventional metasurface approaches, yielding near-unity numerical aperture, a sharp focal point, and efficiencies much higher than those of any state-of-the-art metalens. We design, fabricate, and experimentally test a proof-of-concept hybrid metalens based on this concept, operating in reflection mode. The experimental results are in an excellent agreement with our theory and simulations and clearly validate the superior performance of the proposed design, with efficiencies up to 47.9% and a numerical aperture of 0.98. Although, the proof of concept sample is designed in reflection mode, focusing in one plane, and operating at microwave frequencies, the same concept can be readily applied to higher frequencies and to operate in transmission mode with focus in two dimensions.

Importantly, in our design, we do not perform any overall optimization procedure to maximize the metasurface performance, but simply use the design principles stemming from our analytical approach to gradient metasurfaces and metagratings, approximating locally the metasurface as a fully periodic one. Hence, even improved results may be expected with further optimization. Our results open up opportunities for ultrathin low-weight microwave lenses for communications, radars, and sensing, as well as the possibility of being translated to optics, for nanophotonic and lithography applications.

ACKNOWLEDGMENTS

This work is partially supported by the Air Force Office of Scientific Research, the Department of Defense, the National Science Foundation, and the Simons Foundation.

APPENDIX

As a proof of principle, we design a hybrid metalens for $f = 22.4\,\text{GHz}$; however, the proposed concept can be applied to other portions of the frequency spectrum. In the

following, we provide the design parameters for the proof of concept hybrid metalens. Furthermore, we study the sensitivity of the lens performance to deviations in angle and frequency of the incident wave.

APPENDIX A: ELEMENT DESIGN FOR GRADIENT METASURFACE REGION

The gradient metasurface region of the hybrid metalens is designed according to the required gradient phase profile at the corresponding position, $\Phi = (2\pi/\lambda)\left(\sqrt{x^2 + l_{\mathrm{foc}}^2} - l_{\mathrm{foc}}\right)$. This continuous phase profile is realized using a discrete set of unit cells, each of which is responsible for providing a phase shift sampled on this continuous phase profile. The size of each unit cell is $c_x \times c_y$. To realize these unit cells, we use the design data shown in Fig. 5. To design each building block, we put it in a periodic boundary condition and optimize the element in such a way that it fully reflects the normally incident wave in the specular direction with a required phase (that depends on the location of the unit cell over the surface). We use the frequency domain solver of the CST Microwave studio with the unit-cell boundary conditions. The infinite periodic surface is excited with a y polarized normally incident wave. After designing this infinite surface, we implement each unit-cell design at the corresponding location on the surface of the lens. Notably, due to space limitations, we cannot use more than one unit cell from each kind on the design of the lens. The geometrical parameters for different design points are provided in Fig. 5 together with the phase response for each point. In Fig. 4, we compare fully gradient lenses with metalenses of the same size. The table in Fig. 5 provides the dimensions of the elements for gradient metasurfaces. Gradient metasurfaces with different sizes (different NA) use different numbers of these design points. In Fig. 5, the eight design points in orange are those used to design the elements in the gradient region of the hybrid metalens. In all of these designs, we use DiClad 880 as the substrate. The permittivity of the substrate is 2.2 and the loss tangent is about 0.0009. The thickness of the substrate is (2.3 ± 0.1) mm accompanied by copper on both sides with a thickness of 0.07 mm. Notably, all unit cells use the same substrate material with the same height.

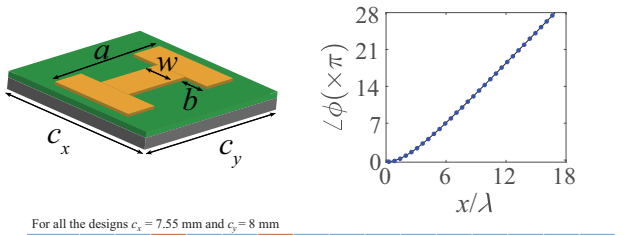

For all the designs c_x = 7.55 mm and c_y = 8 mm

	1st	2nd	3rd	4th	5th	6th	7th	8th	9th	10th	11th	12th	13th	14th	15th
b (mm)	0	0	2.75	0	0	2.75	0	0	0	0	0	0	0	0	0
a (mm)	3.4	2.8	5	5.4	3.8	5	4.5	1	4.9	2.4	5	2.3	4.8	1	4.6
w (mm)	1	1	0.5	1	1	0.5	1	1	1	1	1	1	1	1	1

	16th	17th	18th	19th	20th	21st	22nd	23rd	24th	25th	26th	27th	28th	29th	30th
b (mm)	3	0	2.75	0	1.15	0	0.45	0	0	0	0	3	0	2.45	0
a (mm)	2.5	4.4	5	4.1	6	3.7	6	3.3	5.4	2.4	4.7	2.5	4.3	6	3.9
w (mm)	0.5	1	0.5	1	0.5	1	1	1	1	1	1	0.5	1	0.5	1

FIG. 5. Detailed geometrical parameters for the element design of the gradient metasurface region of the hybrid metalens. Design points in orange are those used for the gradient metasurface region of the hybrid metalens.

APPENDIX B: ELEMENT DESIGN FOR METAGRATING REGION

Besides the gradient metasurface elements, the hybrid metalens design also includes unit cells that are designed based on the metagrating concept. To design these elements, we use the design shown in Fig. 6. The bottom side of the substrate is fully grounded using a thin copper sheet with a thickness of 0.07 mm. Each element is optimized in a unit-cell boundary condition with periodicity $q_x \times q_y$ under a y-polarized normally incident wave. The periodicity of the unit cells are chosen in such a way that ± 1 Floquet channels are open and one of them is aligned towards the focal point (depending on the location of the unit cell on the lens design, these Floquet channels have to be aligned at different directions). The elements are designed so that the infinite periodic surface can fully reflect the normally incident wave into the desired Floquet channel. Notably, the periodicity along y is chosen

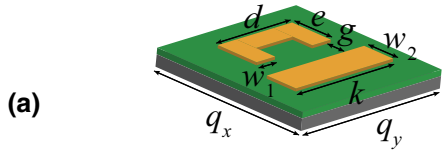

For all the designs q_y = 8 mm and w_1 = 1 mm

	1st	2nd	3rd	4th	5th	6th	7th	8th	9th	10th	11th	12th
q_x (mm)	15.5	14.85	14.45	14.2	14.05	13.92	13.83	13.76	13.72	13.67	13.64	13.61
e (mm)	2	2	2	2.1	2.2	2.4	2.4	2.4	2.4	2.4	2.3	2.3
d (mm)	2.7	2.6	2.6	2.6	2.5	2.4	2.4	2.4	2.4	2.4	2.5	2.5
k (mm)	6.9	4.4	3.7	3.7	3.6	3.6	3.6	3.6	3.6	3.6	3.8	3.8
w_2 (mm)	4.2	4.4	4.5	3.1	2.5	2	1.8	1.7	1.6	1.5	1.5	1.5
g (mm)	0.9	0.6	0.6	0.6	0.6	0.6	0.6	0.6	0.6	0.5	0.5	0.5

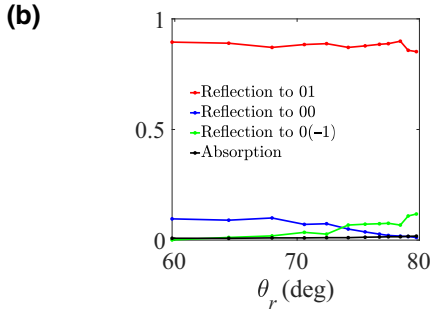

FIG. 6. (a) Detailed geometrical parameters for the design of metagrating elements. (b) Diffraction efficiency in each diffraction channel and absorbed power for each element design.

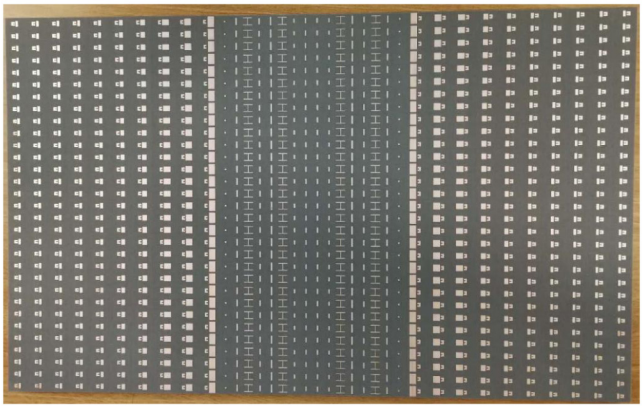

FIG. 7. Fabricated hybrid metalens.

not to allow any higher-order propagating Floquet channel. To engineer unit cells for different design points shown in Fig. 1(c), only the top metallic pattern is optimized, while the substrate material and height remain the same for all unit cells. The detailed structural design parameters are shown in Fig. 6. The absolute diffraction efficiency, with respect to the diffracted angle for different designs, is illustrated in the Fig. 1(c) [see green circles in Figs. 1(c) and 6(b)]. It can be seen that the diffraction efficiency of these infinite surfaces are much higher than those we can obtain using a gradient metasurface [see Fig. 1(c)]. In principle, all of these designs can provide unitary efficiency (for lossless case); however, since in all our numerical simulations we consider realistic material loss, the efficiencies drop slightly. As observed from Fig. 6(b), only 10% of the incident power is lost in the form of scattering into undesired Floquet channels and dissipation due to the realistic loss considered in the designs. After designing the elements one by one, we put one element from each design side by side to create the hybrid metalens. Notably, in the design parameters shows in Fig. 6, the first design is for the closest element to the center of the hybrid metalens and the 12th is the farthest element with respect to the center of the lens.

It should be noted that we do not perform any overall optimization on the whole hybrid metalens for a fair comparison between the proposed hybrid metalens and the conventional gradient lens. Performing an overall optimization and adjustment will increase the efficiency of the design more.

APPENDIX C: MEASUREMENT SETUP

To experimentally validate our design of a hybrid metalens, we fabricate a prototype for operation at 22.4 GHz (see Fig. 7). The same design approach is scalable to different portions of the electromagnetic spectrum, up to the visible range. The dimensions of the fabricated lens are 30.2λ and 18.5λ in the x and y directions, respectively. A WR-42 standard gain horn antenna with a 15 dB nominal gain is used to excite the hybrid metalens. The horn antenna is located 149.3λ away from the fabricated lens to give an incident wave with a reasonably planar wave front at the location of the sample. To capture the performance of the fabricated hybrid metalens, an automated robotic arm scans the space around the focal point enclosed by $\Delta x = 11.2\lambda$ and $\Delta z \approx 3.73\lambda$ on the $y = 0$ plane, with a spatial resolution of 0.07λ [see Fig. 2(b)]. An R&S®ZVA40 vector network analyzer is used to measure the amplitude and phase of the field over the scanning region. To evaluate the reflection from the hybrid metalens, we conduct two measurements. First, we measure the incident field in the absence of the lens $\mathbf{E}_i$ and then we measure the total field, including scattering caused by the focusing lens, $\mathbf{E}_t$.

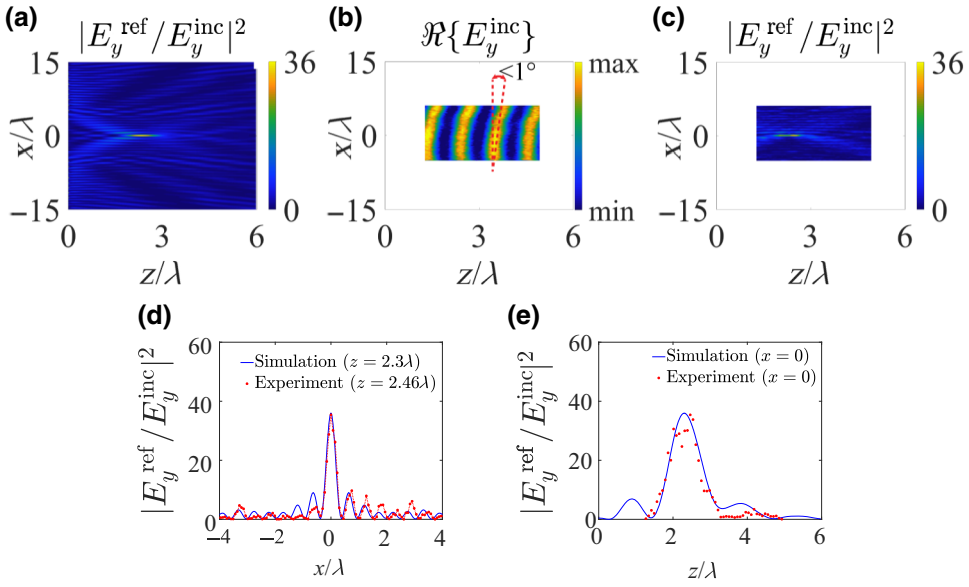

FIG. 8. Numerical and experimental focusing performance of the hybrid metalens at $f_d = 0.94f$ (for this example, $f = 22.4$ GHz). (a) Normalized reflected field intensity (simulation), (b) real part of the incident field in the scanned region (experiment), (c) normalized reflected field intensity in the scanned region (experiment), (d) numerical (solid line) and experimental (dashed lines) reflected field intensity at the position of focal point, and (e) numerical (solid line) and experimental (dashed lines) reflected field intensity along the z direction at $x = 0$.

The scattered field is then obtained as $\mathbf{E}_s = \mathbf{E}_t - \mathbf{E}_i$, normalized to the incident field amplitude. Figures 2(b)–2(d) show the measurement results for the fabricated sample, which verify the theoretical and numerical findings.

APPENDIX D: ANALYZING THE FREQUENCY DISPERSION OF THE HYBRID METALENS

Frequency dispersion is another important factor for the hybrid metalens. In addition to strong spatial dispersion due to the composed grating elements, the metagrating also shows frequency dispersion according to the grating equation, which can affect the focusing behavior. To study this effect, as an example, we study the case of 6% deviation of the illumination wave frequency from the design frequency (i.e., $f_d = 0.94f$, with design frequency $f = 22.4\,\mathrm{GHz}$). Figure 8 represents the simulation and experimental results for this case. As observed, decreasing the frequency brings the focal point closer (i.e., focal distance is 2.3λ in simulation and 2.46λ in measurement) without introducing a dramatic distortion in its field profile. The full width at half maximum of the focusing intensity is $4.8\,\mathrm{mm} = 0.336\lambda$ and the overall focusing efficiency is $\eta = 0.352$, which shows about 10% decrease with respect to the performance at the design frequency.

[1] L. Novotny and B. Hecht, *Principles of Nano-Optics* (Cambridge University Press, Cambridge, England, 2006).

[2] N. Engheta and R. Ziolkowski, *Metamaterials: Physics and Engineering Explorations* (Wiley, New York, 2006).

[3] A. Dhouibi, S. N. Burokur, A. de Lustrac, and A. Priou, Metamaterial-based half Maxwell fish-eye lens for broadband directive emissions, Appl. Phys. Lett. **102**, 024102 (2013).

[4] N. Kundtz and D. R. Smith, Extreme-angle broadband metamaterial lens, Nat. Mater. **9**, 129 (2010).

[5] T. Zentgraf, Y. Liu, M. H. Mikkelsen, J. Valentine, and X. Zhang, Plasmonic luneburg and eaton lenses, Nat. Nanotechnol. **6**, 151 (2011).

[6] A. V. Kildishev, A. Boltasseva, and V. M. Shalaev, Planar photonics with metasurfaces, Science **339**, 1232009 (2013).

[7] N. Yu and F. Capasso, Flat optics with designer metasurfaces, Nat. Mater. **13**, 139 (2014).

[8] S. B. Glybovski, S. A. Tretyakov, P. A. Belov, Y. S. Kivshar, and C. R. Simovski, Metasurfaces: From microwaves to visible, Phys. Rep. **634**, 1 (2016).

[9] N. Yu, P. Genevet, M. A. Kats, F. Aieta, J.-P. Tetienne, F. Capasso, and Z. Gaburro, Light propagation with phase discontinuities: Generalized laws of reflection and refraction, Science **334**, 333 (2011).

[10] S. Sun, K.-Y. Yang, C.-M. Wang, T.-K. Juan, W. T. Chen, C. Y. Liao, Q. He, S. Xiao, W.-T. Kung, G.-Y. Guo, L. Zhou, and D. P. Tsai, High-efficiency broadband anomalous reflection by gradient meta-surfaces, Nano Lett. **12**, 6223 (2012).

[11] M. Kang, T. Feng, H. T. Wang, and J. Li, Wave front engineering from an array of thin aperture antennas, Opt. Express **20**, 15882 (2012).

[12] C. Pfeiffer and A. Grbic, Metamaterial Huygens' Surfaces: Tailoring Wave Fronts with Reflectionless Sheets, Phys. Rev. Lett. **110**, 197401 (2013).

[13] F. Monticone, N. M. Estakhri, and A. Alù, Full Control of Nanoscale Optical Transmission with a Composite Metascreen, Phys. Rev. Lett. **110**, 203903 (2013).

[14] Y. Ra'di, V. S. Asadchy, and S. A. Tretyakov, Tailoring reflections from thin composite metamirrors, IEEE Transactions on Antennas and Propagation **62**, 3749 (2014).

[15] M. Kim, A. M. H. Wong, and G. V. Eleftheriades, Optical Huygens Metasurfaces with Independent Control of the Magnitude and Phase of the Local Reflection Coefficients, Phys. Rev. X **4**, 041042 (2014).

[16] V. S. Asadchy, Y. Ra'di, J. Vehmas, and S. A. Tretyakov, Functional Metamirrors Using Bianisotropic Elements, Phys. Rev. Lett. **114**, 095503 (2015).

[17] L. Lin, X. M. Goh, L. P. McGuinness, and A. Roberts, Plasmonic lenses formed by two-dimensional nanometric cross-shaped aperture arrays for fresnel-region focusing, Nano Lett. **10**, 1936 (2010).

[18] F. Aieta, P. Genevet, M. A. Kats, N. Yu, R. Blanchard, Z. Gaburro, and F. Capasso, Aberration-free ultrathin flat lenses and axicons at telecom wavelengths based on plasmonic metasurfaces, Nano Lett. **12**, 4932 (2012).

[19] X. Ni, S. Ishii, A. V. Kildishev, and V. M. Shalaev, Ultra-thin, planar, Babinet-inverted plasmonic metalenses, Light: Sci. Appl. **2**, e72 (2013).

[20] A. Pors, M. G. Nielsen, R. L. Eriksen, and S. I. Bozhevolnyi, Broadband focusing flat mirrors based on plasmonic gradient metasurfaces, Nano Lett. **13**, 829 (2013).

[21] A. Arbabi, Y. Horie, A. J. Ball, M. Bagheri, and A. Faraon, Subwavelength-thick lenses with high numerical apertures and large efficiency based on high-contrast transmitarrays, Nat. Commun. **6**, 7069 (2013).

[22] M. Khorasaninejad, W. T. Chen, R. C. Devlin, J. Oh, A. Zhu, and F. Capasso, Metalenses at visible wavelengths: Diffraction-limited focusing and subwavelength resolution imaging, Science **352**, 1190 (2016).

[23] S. Vo, D. Fattal, W. V. Sorin, Z. Peng, T. Tran, M. Fiorentino, and R. G. Beausoleil, Sub-wavelength grating lenses with a twist, IEEE Photon. Technol. Lett. **26**, 1375 (2014).

[24] R. Paniagua-Dominguez, Y. F. Yu, E. Khaidarov, R. M. Bakker, X. Liang, Y. H. Fu, and A. I. Kuznetsov, A metalens with near-unity numerical aperture, Nano Lett. **18**, 2124 (2018).

[25] V. S. Asadchy, M. Albooyeh, S. N. Tcvetkova, A. Díaz-Rubio, Y. Ra'di, and S. A. Tretyakov, Perfect control of reflection and refraction using spatially dispersive metasurfaces, Phys. Rev. B **94**, 075142 (2016).

[26] N. M. Estakhri and A. Alù, Wave-Front Transformation with Gradient Metasurfaces, Phys. Rev. X **6**, 041008 (2016).

[27] A. Epstein and G. V. Eleftheriades, Huygens' metasurfaces via the equivalence principle: Design and applications, J. Opt. Soc. Am. B Opt. Phys. **33**, A31 (2016).

[28] Y. Ra'di, D. L. Sounas, and A. Alù, Metagratings: Beyond the Limits of Graded Metasurfaces for Wave Front Control, Phys. Rev. Lett. **119**, 067404 (2017).

[29] H. Chalabi, Y. Ra'di, D. L. Sounas, and A. Alù, Efficient anomalous reflection through near-field interactions in metasurfaces, Phys. Rev. B **96**, 075432 (2017).

[30] A. Epstein and O. Rabinovich, Unveiling the Properties of Metagratings via a Detailed Analytical Model for Synthesis and Analysis, Phys. Rev. Appl. **8**, 054037 (2017).

[31] E. Khaidarov, H. Hao, R. Paniagua-Domínguez, Y. F. Yu, Y. H. Fu, V. Valuckas, S. L. K. Yap, Y. T. Toh, J. S. K. Ng, and A. I. Kuznetsov, Asymmetric nanoantennas for ultrahigh angle broadband visible light bending, Nano Lett. **17**, 6267 (2017).

[32] D. Sell, J. Yang, S. Doshay, R. Yang, and J. A. Fan, Large-angle, multifunctional metagratings based on freeform multimode geometries, Nano Lett. **17**, 3752 (2017).

[33] Y. Ra'di and A. Alù, Reconfigurable metagratings, ACS Photonics **5**, 1779 (2018).

[34] O. Rabinovich and A. Epstein, Analytical design of printed circuit board (PCB) metagratings for perfect anomalous reflection, IEEE Trans. Antennas Propag. **66**, 4086 (2018).

[35] A. M. H. Wong and G. V. Eleftheriades, Perfect Anomalous Reflection with a Bipartite Huygens' Metasurface, Phys. Rev. X **8**, 011036 (2018).

[36] S. J. Byrnes, A. Lenef, F. Aieta, and F. Capasso, Designing large, high-efficiency, high-numerical aperture, transmissive meta-lenses for visible light, Opt. Express **24**, 5110 (2016).